Int J Adv Manuf Technol (2011) 53:81–92
DOI 10.1007/s00170-010-2823-z

ORIGINAL ARTICLE

Study on finish-turning of NiCr20TiAl nickel-based alloy using Al_2O_3/TiN-coated carbide tools

Bin Zou · Ming Chen · Shasha Li

Received: 19 December 2009 / Accepted: 29 June 2010 / Published online: 14 July 2010

Abstract Al_2O_3/TiN-coated tungsten carbide tools were used for finish-turning of NiCr20TiAl nickel-based alloy under various cutting conditions. The cutting forces, surface integrity, and tool wear were investigated, and their formation mechanisms were discussed. The inter-diffusing and transferring of elements between Al_2O_3/TiN-coated tungsten carbide tool and NiCr20TiAl nickel-based alloy were studied during machining. The plastic flow of NiCr20TiAl alloy was present on the machined surface by the lower cutting forces. The flaking of coating and matrix of tools and the heavier plucking and cavities of the machined surface were induced by the higher cutting forces at higher cutting parameters. The tensile residual stress was engendered on the machined surface and increased with the cutting parameters. In view of surface quality and tool wear, the cutting speed of 60 min and feed of 0.15 mm/r are recommended, and depth of cut should not exceed 0.4 mm when Al_2O_3/TiN-coated carbide tools are used for the finish-turning of the NiCr20TiAl alloy.

Keywords NiCr20TiAl · Cutting forces · Surface integrity · Tool wear · Finish-turning

B. Zou
Centre for Advanced Jet Engineering Technologies (CaJET),
School of Mechanical Engineering, Shandong University,
Jinan 250061, People's Republic of China

B. Zou (✉)
Key Laboratory of High Efficiency and Clean Mechanical Manufacture, Ministry of Education, Shandong University,
Jinan 250061, People's Republic of China
e-mail: zou20011110@163.com

M. Chen
School of Mechanical Engineering,
Shanghai Jiao Tong University,
Shanghai 200240, People's Republic of China

S. Li
Lute Technology Development Company,
Shandong Special Equipment Inspection Institute,
Jinan 250013, People's Republic of China

1 Introduction

Nickel-based alloys play an import role in aerospace industry and steam power because they exhibit a good combination of the mechanical properties and heat resistances at high temperature. In order to satisfy the production and integrity requirement of engineering, some alloying elements were added to nickel-based alloys such as Ti and Cr [1]. Some methods of heat treatments such as solution treatment, precipitation treatment, and dispersion hardening treatment were also applied for nickel-based alloys [2]. Nickel-based alloys contain a high percentage of Ni and Cr elements, and a continuous face-centered cubic austenitic phase with poor thermal diffusivity is formed after the solution and precipitation treatments. The austenitic phases contribute to the high yield strength as well as result in the poor machinability of nickel-based alloys. Metal cutting is one of the most important methods of removing unwanted material in the manufacturing of nickel-based alloy parts [2, 3]. However, metal cutting is also a complex process that is involved with the interaction of tools and machined surfaces. The coated tool is one of the important cutting tools for metal cutting and brings a new development to the traditional cemented carbide tool. Because the coated tool had a lower friction coefficient than an uncoated one under similar cutting conditions, it exhibited good cutting performance and economies [4]. Though the coated tool widened the application of cutting

Table 1 The chemical compositions of NiCr20TiAl nickel-based alloy

Chemical composition	C	Si	Mn	P	S	Al	B
Content (wt.%)	0.04–0.10	≤0.30	≤1.00	≤0.010	≤0.010	1.00–1.80	≤0.008
Chemical composition	Cr	Ni	Cu	Co	Ti	Fe	Ti +Al
Content (wt.%)	18.0–21.0	Balance	≤0.20	≤1.00	1.80–2.70	≤1.50	≥3.50

tools in industry, the short tool life and poor surface qualities were still the basic problems in the machining of nickel-based alloys because of a higher chemical activity of nickel-based alloys at higher cutting forces and temperature [5, 6]. Most of the coatings (TiN, TiC, TiCN, and multilayer) had a higher chemical affinity with nickel-based alloys [7, 8]. Thus, the chemical diffusion of the coated tool and machined surface takes place in the machining of nickel-based alloys, which influences the tool life and machined surface quality.

The tool life and wear mechanism in the machining of Inconel 718 were investigated widely by many studies [5, 6, 9, 10]. However, NiCr20TiAl nickel-based alloy is involved with the solution and precipitation treatments in this work and contains a higher percentage of Ni than Inconel 718. This alloy is used for the key parts of the large-scale power steam turbine at an atmosphere with high temperature, high pressure, and water vapor. The surface integrity of alloy parts is important to the performance of the steam turbine. Damages of the machined surface can reduce the wear resistance of part surfaces and result in stress corrosion cracking and distortion of components. Therefore, care must be taken to ensure the surface integrity of components during machining [10, 11]. The cutting tool can alter the quality of the machined surface under optimum cutting conditions [1, 2, 9–12]. Al_2O_3 and TiN have lower conductivity and higher fracture toughness, respectively. Thus, Al_2O_3/TiN coating can protect the tool from thermal damage and improve its wear resistance. The cutting parameters are also important to the metal cutting. Iabal [13] found that the tool–chip contact length varied with the cutting parameters in the turning of AISI 1045 steel and Ti6Al4V and influenced the tool life. Gopalsamy [14] studied the cutting parameters for hard machining through the grey relational theory and ANOVA, and the cutting efficiency was improved in hard machining. In this work, Al_2O_3/TiN-coated WC tools were used for the finish-turning of the NiCr20TiAl alloy under various cutting conditions. The cutting forces, tool wear, and machined surface integrity of NiCr20TiAl alloy were investigated by a dynamometer, scanning electronic microscope (SEM), energy-dispersive spectrometry (EDS), X-ray diffraction analyzer, and inverted metallurgic microscope. Based on these investigations, the mechanisms of tool wear and damages of the machined surface of NiCr20TiAl alloy were discussed. The objective of this work is to provide a combination of the theoretical and practical information for finish-machining of NiCr20TiAl nickel-based alloy.

2 Experimental procedures

The machining material was a NiCr20TiAl nickel-based alloy with solution and precipitation treatments. The chemical composition and mechanical properties of NiCr20TiAl alloy were given in Tables 1 and 2. The cutting tool is Al_2O_3/TiN-coated tungsten carbide prismatic inserts. The whole experimental setup is shown in Fig. 1. The machining trails were carried out on an Index G200 CNC Centre Lathe, employing a continuously variable spindle speed with a range from 20 to 6,000 rpm. The machining bars of NiCr20TiAl alloy had a diameter of 50 mm and length of 300 mm. All the inserts had an identically effective geometry after the rigid clamping in the tool post, i.e., approach angle of 50°, rake angle of 9°, clearance angle of 6°, and nose radius of 0.8 mm. The cutting forces were measured by a Kistler 9272 three-component piezoelectric dynamometer and associated with a 5070 multichannel charge amplifier connected to a PC employing the Kistler force measurement software. Prior to measurement, an approximately 3-mm thickness of the top surface of each bar was removed in order to eliminate any surface defect that affected the measurement results. Each measurement of cutting force was taken using a new insert at the cutting distance of 100 m. The tool wear and machined surface integrity were observed by scanning

Table 2 The mechanical properties of NiCr20TiAl nickel-based alloy

Mechanical properties	Yield strength (MPa)	Tensile strength (MPa)	Elongation (%)	Reduction of area (%)	Impact energy (J)	Hardness (HB)
NiCr20TiAl	≥600	1,000–1,300	≥12	≥12	≥20	310–400

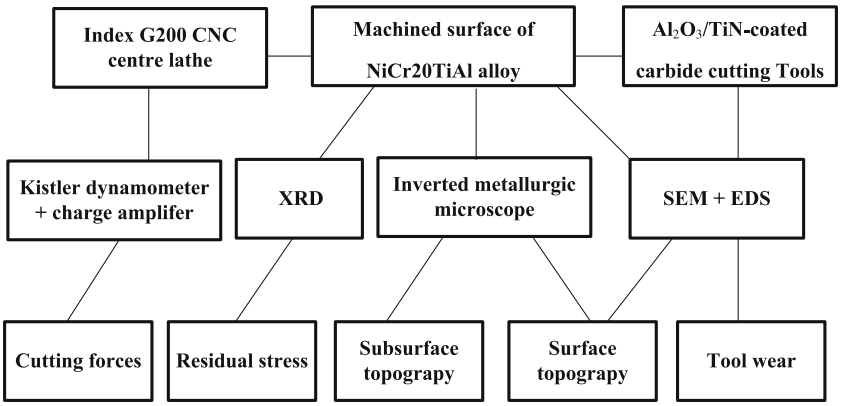

Fig. 1 Diagram of experimental setup for the finish-turning of the NiCr20TiAl alloy

electronic microscope (JEOL JSM-6460, Hitachi, Japan), energy-dispersive spectrometry (PV9900, Philips, Netherlands), and inverted metallurgic microscope. All of the tool wear was observed after a cutting distance of 1 km.

The ideas of the experimental methods for this study were: the full factor experiment including the 18 cutting parameters was designed (cutting speed of 30, 60, and 80 m/min, feed of 0.15 and 0.20 mm/r, and depth of cut of 0.2, 0.4, and 0.6 mm), and all tests were performed under dry conditions. At first, the cutting forces for these 18 cutting parameters were measured, and the effects of the cutting parameters on the cutting forces were investigated. Secondly, the effects of the cutting speed and depth of cut on the surface integrity were investigated. The high cutting speed and depth of cut should be investigated preferentially because they could realize the high cutting efficiency. The cutting parameters that led to the bad surface integrity would be not considered in the subsequent investigation of tool wear. Thirdly, the effects of the cutting parameters on the tool wear were investigated on the premise that these cutting parameters could not cause the very bad surface integrity in the finish-turning of NiCr20TiAl nickel-based alloy. Lastly, based on this analysis, the optimum cutting condition and mechanisms were given.

3 Results and discussion

3.1 Cutting forces

The cutting force was an important factor that influenced the tool wear and machined surface integrity [4, 11]. Figure 2 showed three components of cutting force when NiCr20TiAl nickel-based alloy was turned under various cutting conditions (F_f = feed force, F_p = thrust force, F_c = main cutting force). It was seen from Fig. 2a–c that the main cutting force (F_c) was higher than the thrust force (F_p) and feed force (F_f) at all the cutting conditions. The resultant cutting forces and their three components decreased slightly with an increase of the cutting speed but increased with feed and depth of cut. Shaw [15] found that an increase in the cutting speed caused the cutting temperature to be improved, and the cutting forces were reduced when the cutting temperature reached the softening temperature of workpiece. The main cutting force (F_c) increased more rapidly than feed force (F_f) and thrust force (F_p) when the feed and depth of cut were improved as shown in Fig. 2a–c. Compared with the feed, an increase of the depth of cut led to an obvious improvement of the cutting forces, indicating that the depth of cut had a great effect on the main cutting force. The resultant cutting force reached a maximum value at the cutting speed of 30 m/min, feed of 0.2 mm/r, and depth of cut of 0.6 mm for all testing cutting parameters as shown in Fig. 2d.

3.2 Machined surface quality

3.2.1 Surface topography

At first, the effect of the cutting speed on the surface topography was investigated. Because more cutting heat was generated when the cutting speed was improved [13], the cutting parameters that caused the lower cutting forces should be studied preferentially. According to the cutting forces shown in Fig. 2, two cutting parameters (one is the cutting speed of 30 m/min, feed of 0.15 mm/r, and depth of cut of 0.2 mm; another is the cutting speed of 80 m/min, feed of 0.15 mm/r, and depth of cut of 0.2 m) were studied comparatively. Figure 3 showed the effect of the cutting speed on the machined surfaces topography of NiCr20TiAl alloy (V_c=30 m/min, f=0.15 mm/r, and a_p=0.2 mm as seen in Fig. 4a and V_c=80 m/min, f=0.15 mm/r, and a_p=0.2 mm as seen in Fig. 3b). The plastic flow of the machined surface was observed at the cutting speed of 30 m/min, feed of 0.15 mm/r, and depth of cut of 0.2 mm (seen in Fig. 3a). It was seen from Fig. 3b that there were plucking and sphere particles on the machined surface when the cutting speed was increased from 30 m/min to 80 m/min. EDS analyses were used to examine the marked regions on the

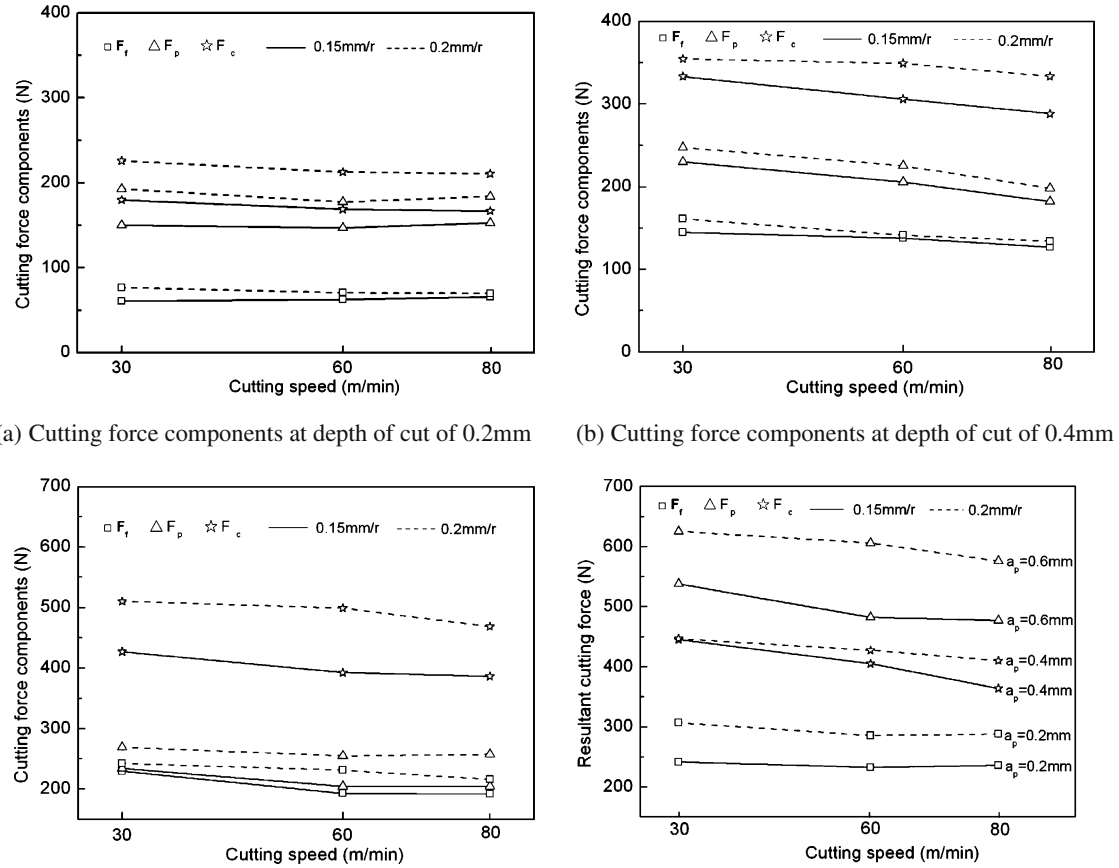

(a) Cutting force components at depth of cut of 0.2mm

(b) Cutting force components at depth of cut of 0.4mm

(c) Cutting force components at depth of cut of 0.6mm

(d) Resultant cutting force in different cutting conditions.

Fig. 2 Cutting forces in the finish-turning of the NiCr20TiAl alloy under various conditions

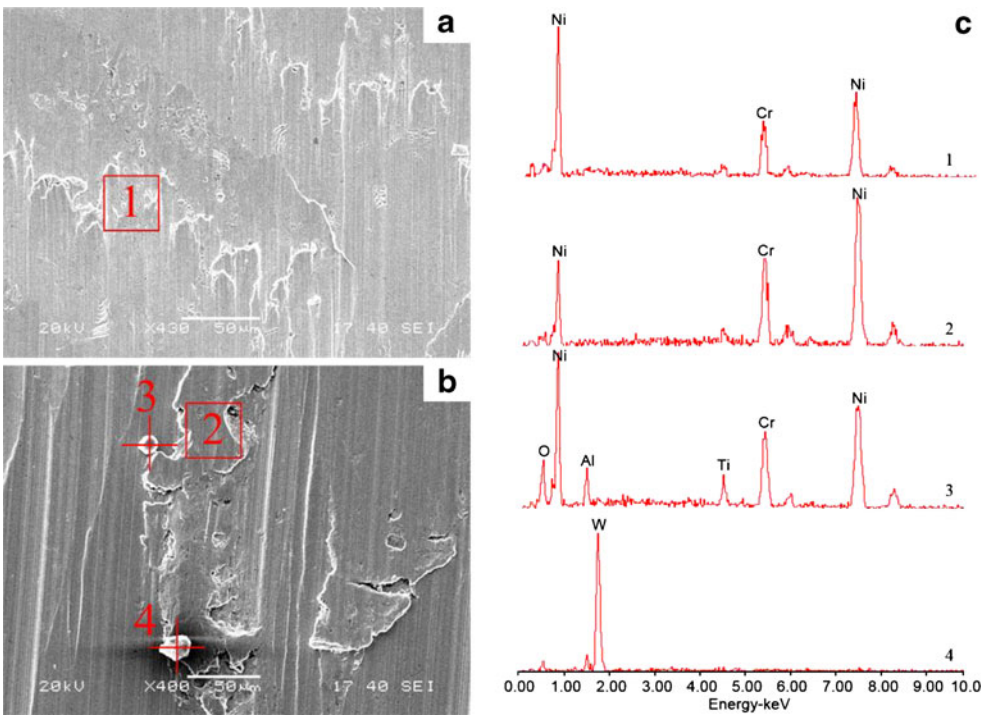

Fig. 3 SEM micrograph of the machined surfaces topography of NiCr20TiAl nickel-based alloy at a **a** cutting speed of 30 m/min, feed of 0.15 mm/r, and depth of cut of 0.2 mm and **b** cutting speed of 80 m/min, feed of 0.15 mm/r, and depth of cut of 0.2 mm, and **c** EDS analysis which detected the marked regions of 1, 2, 3, and 4 on the machined surface of **a** and **b**

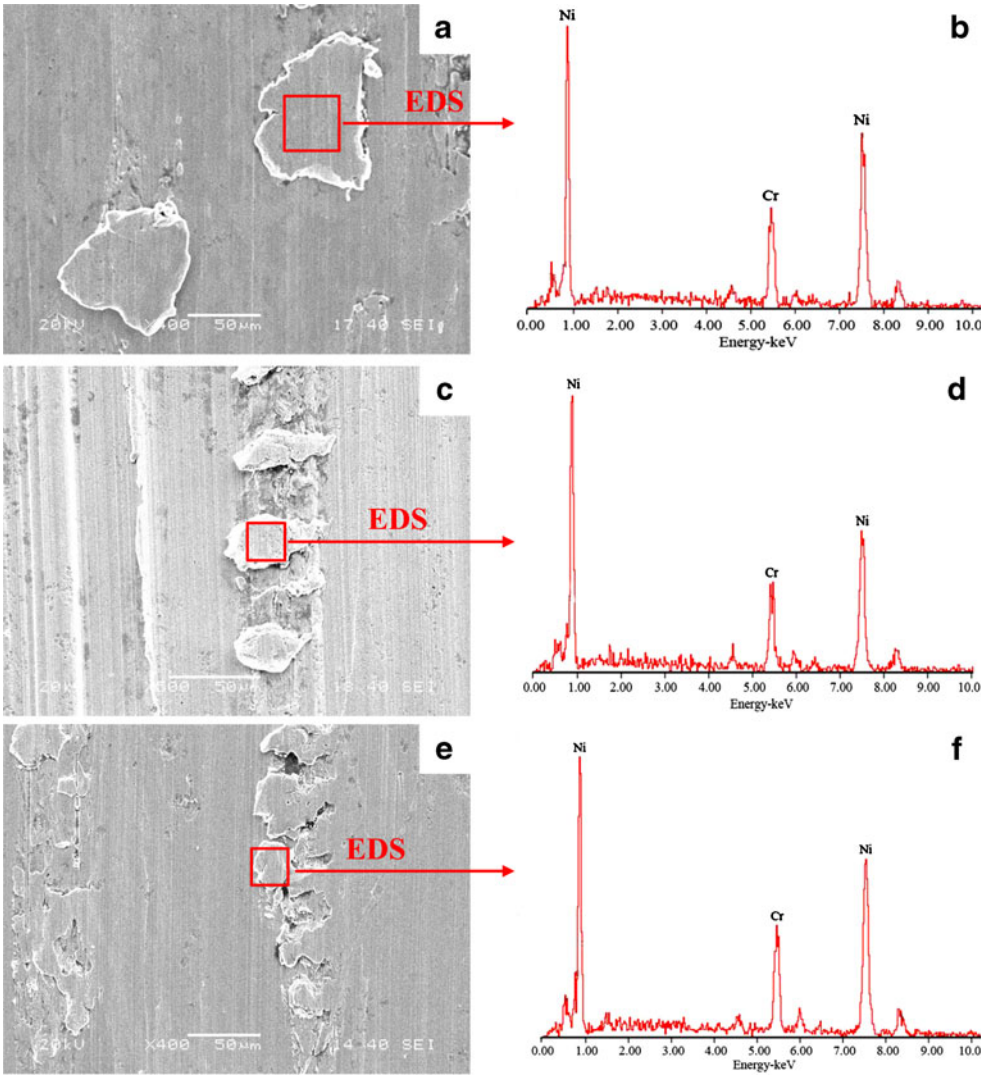

Fig. 4 SEM and EDS micrograph of the machined surface topography of NiCr20TiAl alloy at **a**, **b** the cutting speed of 60 m/min, feed of 0.15 mm/r, and depth of cut of 0.2 mm, **c**, **d** the cutting speed of 60 m/min, feed of 0.15 mm/r, and depth of 0.4 mm, and **e**, **f** the cutting speed of 60 m/min, feed of 0.15 mm/r, and 0.6 mm

machined surfaces in Fig. 3a, b. Curve 1 of EDS (seen in Fig. 3c) revealed that it contained a higher percentage of Ni and Cr in the zones of plastic flow. This indicated that no elements of the tool adhered to the machined surface at the cutting speed of 30 m/min, feed of 0.15 mm/r, and depth of cut of 0.2 mm. EDS analyses also confirmed that the components of plucking in region 2 (seen in Fig. 3b) were consistent with those in region 1 (seen in Fig. 3a). Ti and Al were contained beside Ni and Cr in region 3 and the sphere particle in region 4 was a tungsten compound (seen in Fig. 3b, c). The plastic flow and plucking of the machined surface were ascribed to the higher strength and plasticity of NiCr20TiAl alloy as well as the cutting forces. Many studies found that the higher cutting speed induced the higher cutting temperature and thermal softening of the machined surface [15, 16]. Therefore, the machined surface was subject to plastic flow and plucking in Fig. 3b. The sphere particles on the machined surface were the coating and substrate of the tool because a high percentage of Ti, Al, and W were identified by curve 3 of EDS (seen in Fig. 3c). At higher cutting speed, the coating and substrate were flaked from the tool and adhered to the machined surface due to the higher cutting temperature. Thus, it was suggested that the cutting speed of 80 m/min could not be adopted in the finish-turning of the NiCr20TiAl alloy using Al_2O_3/TiN-coated tungsten carbide tools.

Secondly, the effect of the depth of cut on the surface topography was studied. According to the cutting forces shown in Fig. 2, there cutting parameters (the depth of cut of 0.2, 0.4, and 0.6 mm at the cutting speed of 60 m/min and feed of 0.15 m/min) were investigated comparatively. Figure 4 showed that the effect of the depth of cut on the machined surfaces topography of NiCr20TiAl alloy (V_c= 60 m/min, f=0.15 mm/r, and a_p=0.2 mm in Fig. 4a, b, V_c= 60 m/min, f=0.15 mm/r, and a_p=0.4 mm in Fig. 4c, d, and V_c=60 m/min, f=0.15 mm/r, and a_p=0.6 mm in Fig. 4e, f). When the depth of cut increased, many plucking were generated on the machined surface, but the volume of

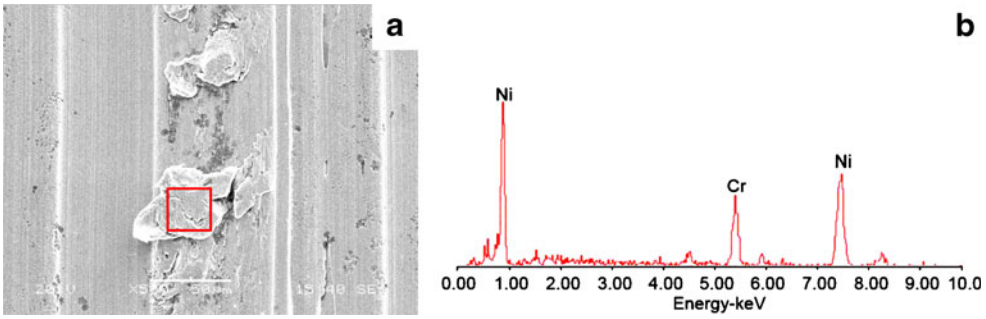

Fig. 5 **a** SEM micrograph of the machined surface topography of NiCr20TiAl nickel-based alloy at the cutting speed of 60 m/min, feed of 0.2 mm/r, and depth of cut of 0.2 mm and **b** EDS analysis which detected the marked regions on the machined surface of **a**

plucking became small. The EDS observations showed that these plucking belonged to the workpiece material. At the depth of 0.6 mm (seen in Fig. 4c), the severe plastic plow and many plucking were caused on the machined surface. However, the quantity of plucking was relatively small at the depth of 0.2 and 0.4 mm. Thus, the depth of 0.6 mm was not recommended in the finish-turning of the NiCr20-TiAl alloy using Al_2O_3/TiN-coated carbide tools.

Thirdly, the effect of feed on the surface topography was investigated in Figs. 4, 5, 6, and 7. Compared with Fig. 4a, b (V_c=60 m/min, f=0.15 mm/r, and a_p=0.2 mm), Fig. 5 showed SEM micrograph and EDS analyses of the machined surface topography at the cutting speed of 60 m/min, feed of 0.2 mm/r, and depth of cut of 0.2 mm. It was seen from Fig. 5a that the small plucking was present on the machined surface of the NiCr20TiAl alloy. The EDS analysis (seen in Fig. 5b) revealed that these plucking contained a higher percentage of Ni and Cr, indicating that no tool material adhered to the machined surface. Compared with the cutting condition (f=0.15 mm/r and a_p= 0.2 mm), the increased cutting forces (V_c=60 m/min, f= 0.2 mm/r, and a_p=0.2 mm) contributed to these plucking. Our previous work had demonstrated that surface plucking was related with the plastic flows and cavities of machined surface when NiCr20TiAl alloy was cut by the uncoated tools [17]. However, the higher cutting forces urged more serious plastic flow to occur, and the plastic flow was converted into the plucking of the machined surface as the cutting shear stress exceeded the tensile strength of the NiCr20TiAl alloy. Some materials were removed with chips and others adhered onto the machined surfaces to become plucking. Compared with Fig. 4c, d (V_c=60 m/min, f= 0.15 mm/r, and a_p=0.4 mm), Fig. 6 showed SEM micrographs and EDS analyses of the machined surface topog-

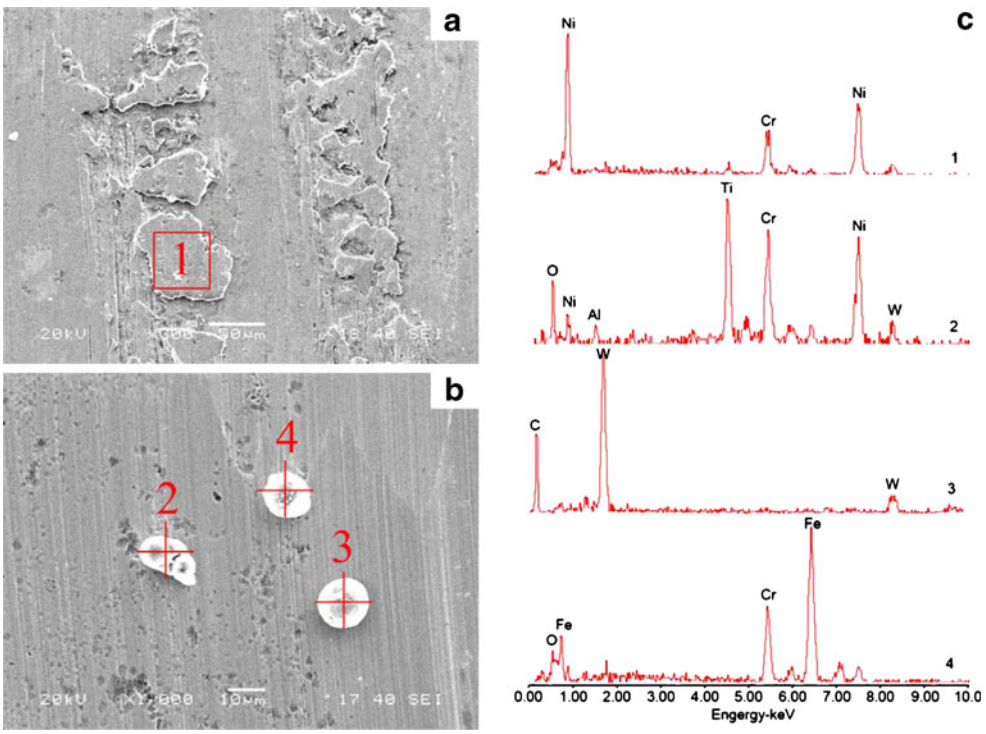

Fig. 6 **a** SEM micrograph of the machined surface topography of NiCr20TiAl nickel-based alloy at the cutting speed of 60 m/min, feed of 0.2 mm/r, and depth of cut of 0.4 mm and **b** EDS analysis which detected the marked regions s of 1, 2, 3, and 4 on the machined surface of **b** and **c**

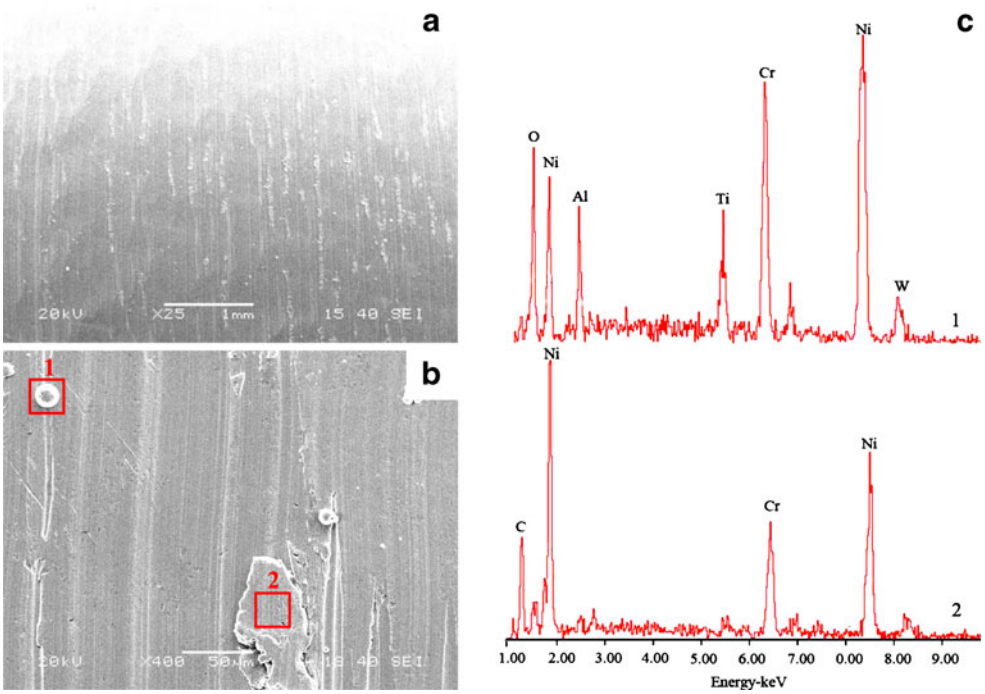

Fig. 7 **a**, **b** SEM micrograph of the machined surface topography of NiCr20TiAl alloy at the cutting speed of 60 m/min, feed of 0.2 mm/r, and depth of cut of 0.6 mm and **c** EDS analysis which detected the marked regions s of 1 and 2 on the machined surface of **b**

raphy at the cutting speed of 60 m/min, feed of 0.2 mm/r, and depth of cut of 0.4 mm. The cutting force at the depth of cut of 0.4 mm was twice as much as that of 0.2 mm in Fig. 2, and this resulted in the different machined surface topography. It was seen from Fig. 6a that a great deal of surface plucking with the short spacing intervals was distributed on the machined surface. It indicated that the heavy interaction of tool and machined surface generated more surface plucking. The surface plucking could lead to the catastrophic fracture of the insert edge in the further machining [11, 18]. Besides surface plucking, many different sphere particles were found on the machined surface, and three representative particles were given at a higher magnification (seen in Fig. 6b, c). Particle 2 in Fig. 6b was different from surface plucking in Fig. 6a and contained a higher percentage of Ti, Al, and O. Particle 3 in Fig. 6b was a tungsten carbide compound. These two kinds of particles (particles 2 and 3) were derived from the tool. The third kind of particles was also observed on the machined surface (particle 4 in Fig. 6b), and EDS analyses indicated that it was a ferrous compound. This ferrous compound on the machined surface was related to the cutting temperature. Investigations on the cutting temperature [4, 9, 12] showed that temperature in the cutting area was much higher in the machining of nickel-based alloys than the conventional steels at the higher cutting parameters. The higher cutting temperature made some elements of NiCr20TiAl alloy to be oxidized into oxides. However, these particles usually had a higher hardness and could score the machined surface, which was detrimental to the wear and corrosion resistances of the machined surface. Figure 7 shows SEM micrographs and EDS analyses of the machined surface topography at the cutting speed of 60 m/min, feed of 0.2 mm/r, and depth of cut of

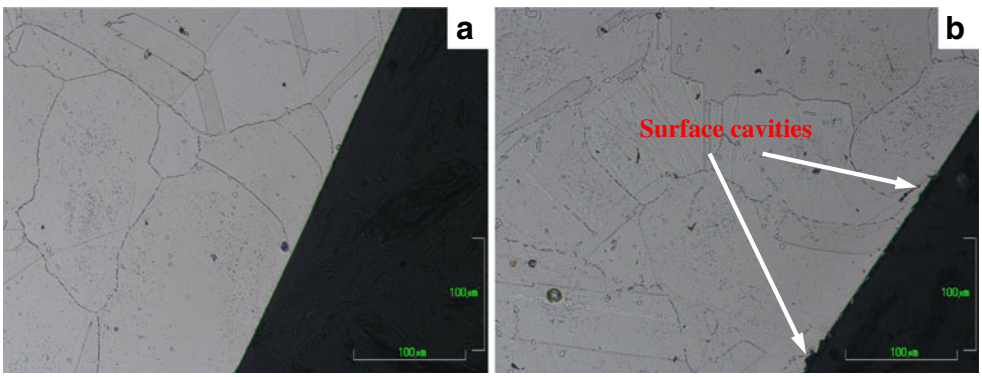

Fig. 8 Metallographic micrograph of cross-section of the machined surface after the NiCr20TiAl alloy was turned **a** at the cutting speed of 60 m/min, feed of 0.15 mm/r, and depth of cut of 0.2 mm and **b** at the cutting speed of 80 m/min, feed of 0.15 mm/r, and depth of cut of 0.2 mm

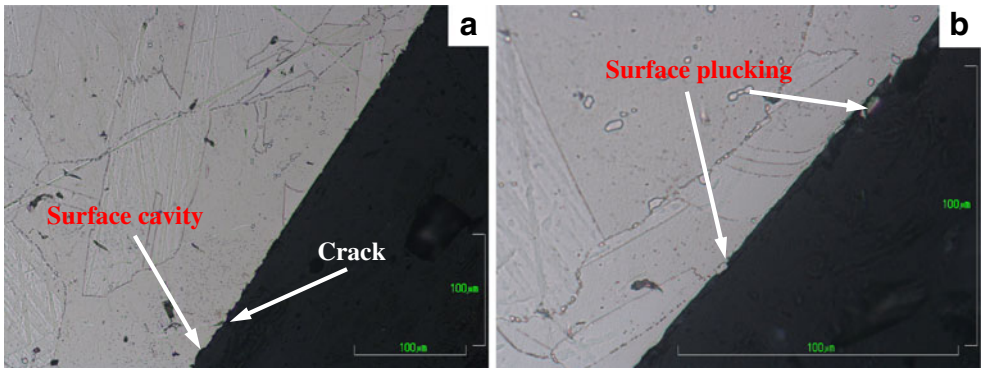

Fig. 9 Metallographic micrograph of cross-section of the machined surface after NiCr20TiAl alloy was turned at the cutting speed of 60 m/min, feed of 0.2 mm/r, and depth of cut of 0.2 mm: **a** surface cavities and crack and **b** surface plucking

0.6 mm. The cutting forces at the depth of cut of 0.6 mm were much higher than 0.4 mm in Fig. 2. The higher cutting forces gave rise to a cutting vibration of machines and clamping fixtures during machining. This made the cut condition vary with the cutting vibration during machining. The machined surface topography with many chatter marks (seen in Fig. 7a) resulted from the cutting vibration. Some surface plucking and sphere particles were also found on the machine surface (seen in Fig. 7b). According to Figs. 4, 5, 6, and 7, the depth of 0.4 and 0.6 mm was not recommended if the feed of 0.2 mm/r was adopted.

3.2.2 Subsurface topography

The subsurface topography was observed on the cross-section of the machined surface by the metallurgic microscope. Figure 8 showed the metallographic micrograph of cross-section of the machined surface after NiCr20TiAl alloy was turned at: (a) the cutting speed of 60 m/min, feed of 0.15 mm/r, and depth of cut of 0.2 mm and (b) the cutting speed of 80 m/min, feed of 0.15 mm/r, and depth of cut of 0.2 mm. The machined surface was very straight on the cross-section view in Fig. 8a. Some smaller cavities were induced in the subsurface when the cutting speed was increased to 80 m/min in Fig. 8b. A metallographic micrograph of the subsurface is shown in Fig. 9 after the NiCr20TiAl alloy was turned at the cutting speed of 60 m/min, feed of 0.2 mm/r, and depth of cut of 0.2 mm. The smaller surface cavities and cracks were found in the subsurface as shown in Fig. 9a and surface plucking was present on the machined surface as shown in Fig. 9b. The surface cavities and cracks in the subsurface were related with the plucking on the machined surface. If the plucking was removed from the machined surface, some materials were pulled out from the machined surface, and then cavities and cracks were left in the subsurface. Figure 10 shows the metallographic micrograph of subsurface after NiCr20TiAl alloy was turned at the cutting speed of 60 m/min, feed of 0.2 mm/r, and depth of cut of 0.2 mm. Some bigger surface cavities were generated in the subsurface (seen in Fig. 10a). According to the machined surface as shown in Fig. 6a, the bigger plucking was present on the machined surface. If the bigger plucking was removed from the machined surface, some pull-off plucking formed the bigger cavities in the subsurface. The grains of NiCr20TiAl alloy were distorted severely and some dislocations piled up in Fig. 10b. The subsurface damages of NiCr20TiAl alloy resulted from the higher cutting forces at the cutting speed of 60 m/min, feed of 0.2 mm/r, and depth of cut of

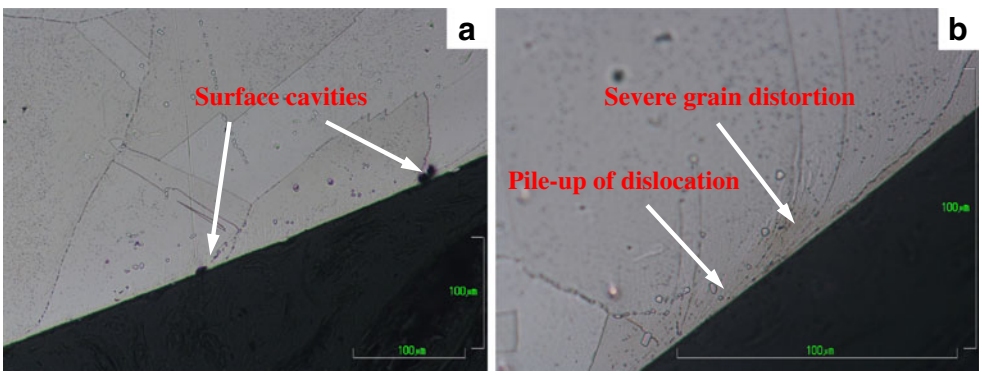

Fig. 10 Metallographic micrograph of cross-section of the machined surface after NiCr20-TiAl alloy was turned at the cutting speed of 60 m/min, feed of 0.2 mm/r, and depth of cut of 0.4 mm: **a** surface cavities and **b** severe grain distortion and pile-up of dislocation

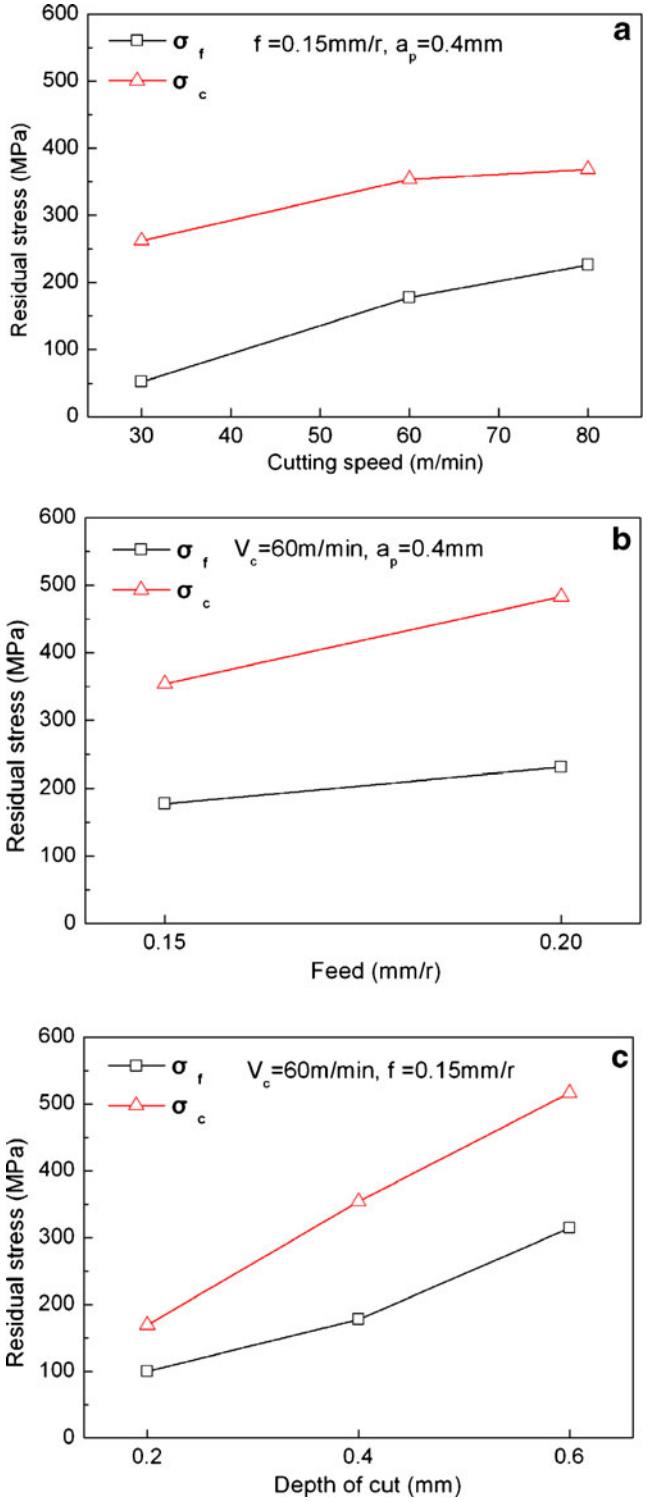

Fig. 11 Residual stress of machined surface induced by the interaction of Al_2O_3/TiN-coated WC tool and machined surface of NiCr20TiAl alloy in the various cutting conditions. σ_c and σ_f denote the residual stresses along the cutting direction and feed direction, respectively

0.4 mm. However, these damages do not have a good effect on the quality and performance of the machined surface quality. Therefore, for the subsurface of the NiCr20TiAl alloy after the finish-machining, the depth of cut should not exceed 0.4 mm.

3.2.3 Residual stress

The residual stress of machined surface caused by the finish-turning of the NiCr20TiAl alloy is given in Fig. 11. It can be seen that the depth of cut had a greater influence on the residual stress of the machined surface than the cutting speed and feed. As the depth of cut was increased, the tensile residual stress was improved rapidly as shown in Fig. 11c. Especially the residual stress was enhanced by approximate three times at the depth of cut of 0.6 than 0.2 mm. For all the cutting conditions in this work, the tensile residual stress of the machined surface was produced (no compressive residual stress was found), and there was no drop in the residual stress when increasing the cutting speed and feed. It was not in agreement with Wardany [20] who found that an increase of the cutting speed could reduce the tensile residual stress because of the increased chip flow rate, and an improvement of the feed could result in a trend toward the higher compressive stress. In our work, increasing the cutting speed gave rise to an improvement of the tensile residual stress even if the cutting forces decreased slightly. However, the residual stress state of the machined surface after machining was a combination of the effects of the thermal and mechanical loads [10]. Especially the thermal load was responsible for the tensile residual stress of the machined surface. Furthermore, the coating of the tool had a strong effect on the

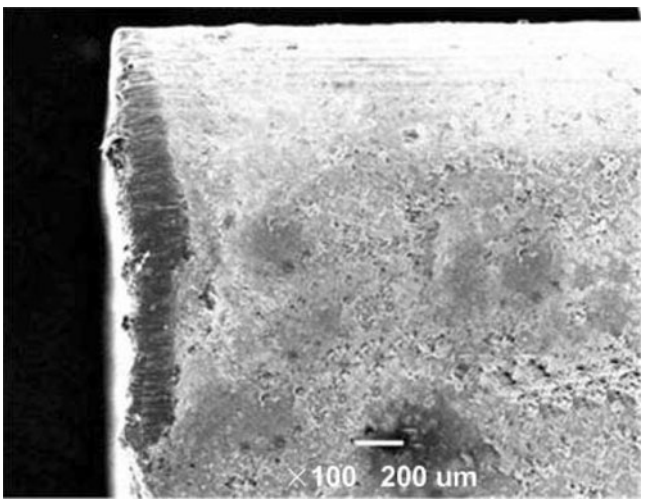

Fig. 12 SEM micrograph of flank wear of Al_2O_3/TiN-coated WC tool at the cutting speed of 60 m/min, feed of 0.15 mm/r, and depth of cut of 0.2 mm

thermal load on the machined surface. During machining, the multilayer Al_2O_3/TiN coatings could prevent the cutting heat dissipating into the bulk of the tool due to the lower conductivity of Al_2O_3 (as the thermal barrier layer on the surface of tool [21]). An amount of heat is centralized at the contact area and induced the higher tensile stress to be improved. However, for the cutting conditions (one is cutting speed of 60 m/min, feed of 0.2 mm/r, and depth of cut of 0.6 mm; another is cutting speed of 60 m/min, feed of 0.2 mm/r, and depth of cut of 0.4 mm), the residual stress in the direction of cutting speed approached to the yield strength of the NiCr20TiAl alloy at the depth of 0.6 mm. Therefore, in view of the residual stress, the depth of 0.6 mm or feed of 0.2 mm/r was not recommended when Al_2O_3/TiN-coated WC tool was used in the finish-turning of the NiCr20TiAl alloy.

3.3 Tool wear

At the cutting speed of 60 m/min, feed of 0.15 mm/r, and depth of cut of 0.2 mm, a non-uniform wear was dominated as shown in Fig. 12. The maximum of tool wear approaches to 0.25 mm. Figure 13 showed the SEM micrographs and EDS analyses of tool wear at the cutting speed of 60 m/min, feed of 0.15 mm/r, and depth of cut of 0.4 mm. It was seen from Fig. 13 that the cutting tool edge was worn out and some materials adhered to the worn tool. An EDS detector was used to examine two regions of the tool flank (regions A and B in Fig. 2). Region A was an unworn one and EDS analyses showed that the coating of the tool consisted of Ti and Al. Region B was a worn one including Ni and Cr as shown by EDS analyses, indicating that there was a strong chemical affinity of the NiCr20TiAl alloy with the tool during finish-machining. Wang and Ezugwu [19, 21] considered that the adhesive workpiece materials remained on the tool in the cutting process. Before the adhesive stress reached a sufficiently high level to detach it from the reaction layer, this diffusion layer could inhibit the transport of tool material into workpieces and reduce the rate of tool wear to a certain extent. However, the adhesive layer would cause the quick tool wear if it detached from the tool in machining. In this work, the high affinity of Ni and Cr (in the NiCr20TiAl alloy) with W and Ti (in the Al_2O_3/TiN-coated WC tool) induced the formation of the adhesive layer containing Ni and Cr on the worn tool during machining, but a crack was found in the adhesive layer of the worn tool (seen in Fig. 13), which meant that the adhesive layer would be detached from the tool if the tool continued to cut the NiCr20TiAl alloy. However, the tool wear was acceptable at the cutting speed of 60 m/min, feed of 0.15 mm/r, and depth of cut of 0.4 mm because it did not exceed 0.3 mm after a cutting distance of 1 km.

Figure 14a, b shows SEM micrographs of the worn tool at the cutting speed of 60 m/min, feed of 0.2 mm/r, and depth of cut of 0.4 mm and the cutting speed of 60 m/min, feed of 0.2 mm/r, and depth of cut of 0.6 mm, respectively.

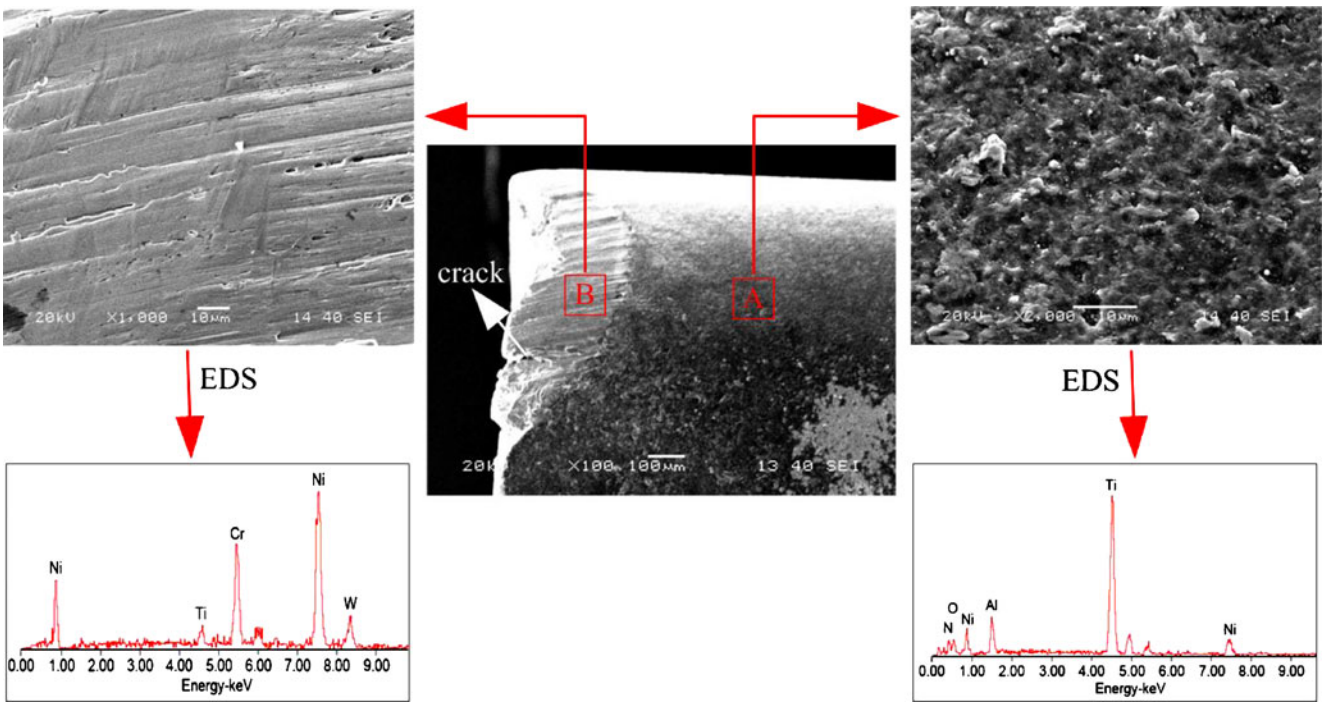

Fig. 13 SEM and EDS analyses of flank wear of Al_2O_3/TiN-coated WC tool at the cutting speed of 60 m/min, feed of 0.15 mm/r, and depth of cut of 0.4 mm

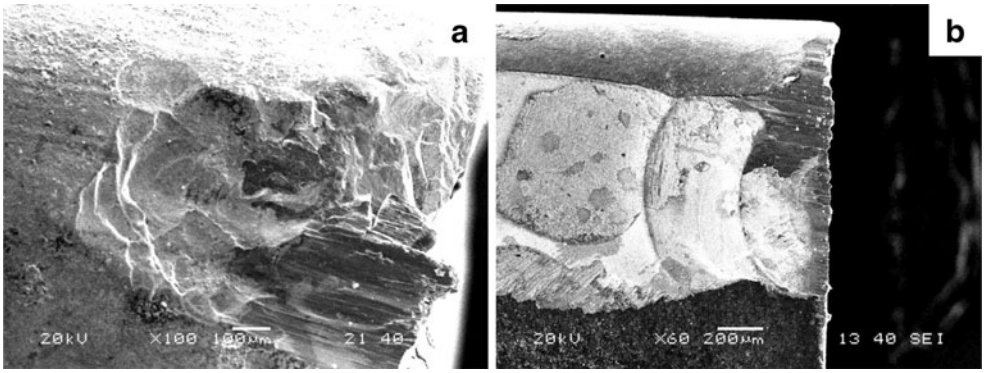

Fig. 14 SEM micrograph of flank wear of Al_2O_3/TiN-coated WC tool at **a** the cutting speed of 60 m/min, feed of 0.2 mm/r, and depth of cut of 0.4 mm and **b** the cutting speed of 60 m/min, feed of 0.2 mm/r, and depth of cut of 0.6 mm

It was seen from Fig. 14 that some cracks were generated on the worn tool and that tool breakage took place. However, the higher cutting force was liable to encourage the vibration of the machining system and caused the tool to undergo an alternate stress with high frequency at a higher cutting speed. It was responsible for the tool breakage. However, the tool breakage during machining had a more severe influence on the machined surface topography. Thus, the depth of 0.6 mm or feed of 0.2 mm/r could hardly be adopted due to the heavy tool wear in the finish-turning of the NiCr20TiAl alloy.

4 Conclusion

Al_2O_3/TiN-coated tungsten carbide tools were used for the finish-turning of the NiCr20TiAl nickel-based alloy under various conditions. The following conclusions are derived from this investigation:

1. The cutting forces decreased slightly with an increase of the cutting speed and increased with feed and depth of cut. The depth of cut had a great effect on the increase of cutting forces.
2. In the finish-turning of the NiCr20TiAl alloy, the plastic flow of the machined surface was produced at a low cutting speed. The increased cutting forces urged the plastic flow to be converted into plucking. At higher cutting speed and depth of cut, a great deal of surface plucking, coating, and matrix of tool and ferrous compounds were produced on the machined surface of NiCr20TiAl alloy. The chemical diffusion happened when Al_2O_3/TiN-coated WC tool was used for the finish-turning of the NiCr20TiAl alloy. Due to the strong bonding between the tool and the adhesive layers, some substrate and coating particles were detached from the tool and attached onto the machined surfaces of the NiCr20TiAl alloy.

Few damages happened in the subsurface at the lower cutting speed and depth of cut. Some bigger surface cavities, severe grain distortion, and pile-up of dislocation were generated in the subsurface at the higher feed and depth of cut. If the bigger plucking was removed from the machined surface, some pull-off plucking formed the bigger cavities in the subsurface. However, these serious subsurface damages resulted from the higher cutting forces and had a bad effect on the quality and performance of the machined surface quality.Increasing the cutting speed gave rise to an improvement of the tensile residual stress. No compressive residual stress was found on the machined surface. The residual stress in the direction of cutting speed approached to the yield strength of the NiCr20TiAl alloy at the depth of 0.6 mm.

3. During the finish-turning of the NiCr20TiAl alloy, Ni and Cr of the NiCr20TiAl alloy adhered to the tool because of a strong chemical affinity of the NiCr20TiAl alloy with the Al_2O_3/TiN-coated tool. The adhesive layer could inhibit the diffusion of tool material as a diffusion boundary and reduce the rate of tool wear to a certain extent, but the quick tool wear was induced if the adhesive layer was detached from the tool. The tool breakage happened at the depth of cut in excess of 0.4 mm because the higher cutting forces encouraged the vibration of the machining systems. However, the tool wear was acceptable at the cutting speed of 60 m/min, feed of 0.15 mm/r, and depth of cut of 0.4 mm because it did not exceed 0.3 mm after a cutting distance of 1 km.
4. In view of surface quality and tool wear, the cutting speed of 60 m/min and feed of 0.15 mm/r were recommended, and depth of cut should not exceed 0.4 mm when Al_2O_3/TiN-coated carbide tools are used for the finish-turning of the NiCr20TiAl alloy.

Acknowledgements This work is supported by the National Natural Science Foundation of China (No.50935001, No.U0734007), Independent Innovation Foundation of Shandong University, IIFSDU (No. 2009TS029), Important National Science & Technology Specific Projects (2009ZX04014-041), and National 863 project (2009AA04Z150).

References

1. Ezugwu EO, Wang ZM, Machado AR (1996) The machinability of nickel-based alloy: a review. J Mater Process Technol 86:1–16
2. Raman S, Longstreet A, Guha D (2002) A fractal view of tool–chip interfacial friction in machining. Wear 253:1111–1120
3. Abdel HA, Nouari M, Mansori ME (2009) Tribo-energetic correlation of tool thermal properties to wear of WC-Co inserts in high speed dry machining of aeronautical grade titanium alloys. Wear 266:432–443
4. Ghani JA, Choudhury IA, Masjuki HH (2004) Wear mechanism of TiN coated carbide and uncoated cermets tools at high cutting speed application. J Mater Process Technol 153–154:1067–1073
5. Jawaid A, Koksal S, Sharif S (2001) Cutting performance and wear characteristics of PVD coated and uncoated carbide tools in face milling Inconel 718 aerospace alloy. J Mater Process Technol 116:2–9
6. Kitagawa T, Kubo A, Maekawa K (1997) Temperature and wear of cutting tools in high-speed machining of Inconel 718 and Ti–6Al–6V–2Sn. Wear 202:142–148
7. Lim CY, Lau PP, Lim SC (2001) Work materials and the effectiveness of coated tools. Surf Coat Technol 146–147:298–304
8. Klocke F, Krieg T (1999) Coated tools for metal cutting—features and applications. CIRP Ann 48:515–525
9. Krain HR, Sharman AR, Ridgway K (2007) Optimisation of tool life and productivity when end milling Inconel 718TM. J Mater Process Technol 189:153–161
10. Sharman AR, Hughes JI, Ridgway K (2007) An analysis of the residual stresses generated in Inconel 718^{TM} when turning. J Mater Process Technol 173:359–367
11. Devillez A, Schneider F, Dominiak S, Dudzinski D, Larrouquere D (2007) Cutting forces and wear in dry machining of Inconel 718 with coated carbide tools. Wear 262:931–942
12. Hua J, Shivpuri R, Cheng XM, Bedekar V, Matsumoto Y, Hashimoto F (2005) Effect of feed rate, workpiece hardness and cutting edge on subsurface residual stress in the hard turning of bearing steel using chamfer+hone cutting edge geometry. Mater Sci Eng 394:238–248
13. Iqbal SA, Mativenga PT, Sheikh MA (2009) A comparative study of the tool–chip contact length in turning of two engineering alloys for a wide range of cutting speeds. Int J Adv Manuf Technol 42:30–40
14. Gopalsamy BM, Mondal B (2009) Optimisation of machining parameters for hard machining: grey relational theory approach and ANOVA. Int J Adv Manuf Technol 45:1068–1086
15. Shaw MC (2005) Metal cutting principle. Oxford, New York
16. Ezugwu EO, Bonney J, Olajire KA (2004) The effect of coolant concentration on the machinability of nickel-based nimonic C-263 alloy. Tribol Lett 16:311–316
17. Zou B, Chen M, Huang CZ, An QL (2009) Study on surface damages caused by turning NiCr20TiAl nickel-based alloy. J Mater Process Technol 209:5802–5806
18. Rao PN (2005) Manufacturing technology—metal cutting & machine tools. China Machine, Beijing
19. Wang ZG, Wong YS, Rahman M (2005) High-speed milling of titanium alloys using binderless CBN tools. Int J Mach Tools Manuf 45:105–114
20. EI-Wardany TI, Kishawy HA, Elbestawi MA (2000) Surface integrity of die material in high speed machining. Part 2: microhardness variations and residual stress. Transact ASME J Manuf Sci Eng 122:632–641
21. Ezugwu EO, Bonney J, Yamane Y (2003) An overview of the machinability of aeroengine alloys. J Mater Process Technol 134:233–253